Available online at www.sciencedirect.com

ScienceDirect

Proceedings of the Combustion Institute 38 (2021) 5181–5190

Proceedings of the Combustion Institute

www.elsevier.com/locate/proci

The blow-off and transient characteristics of co-firing ammonia/methane fuels in a swirl combustor

Meng Zhang [a,*], Xutao Wei [a], Jinhua Wang [a], Zuohua Huang [a], Houzhang Tan [b]

[a] State Key Laboratory of Multiphase Flow in Power Engineering, Xi'an Jiaotong University, Xi'an 710049, China
[b] MOE Key Laboratory of Thermo-Fluid Science and Engineering, Xi'an Jiaotong University, Xi'an 710049, China

Received 7 November 2019; accepted 21 August 2020
Available online 7 October 2020

Abstract

Recent studies have demonstrated that ammonia could be one of the most promising hydrogen carrier candidates which can be used in large-scale power plants. However, it is challenging to burn ammonia in gas turbines due to its narrow flame stabilization limits. This study investigates the blow-off characteristics and flame macrostructure transition behavior of ammonia/air flame (i.e. NH_3 flame) and ammonia/methane/air flame (i.e. 50%NH_3 flame) in a swirl combustor. Methane/air flame (i.e. CH_4 flame) is also demonstrated for comparative purposes. The flow field and instantaneous OH profile are measured with PIV and OH-PLIF technique, respectively. Large eddy simulation (LES) is conducted to extend understandings of the experimental findings. The results show that the NH_3 flame possesses a poor lean flame stability limit which can be largely extended by adding CH_4 in the fuel. Moreover, changing swirl number (S) shows no apparent effect on the lean blow-off limit (ϕ_b) for the NH_3 flame. On the contrary, a clear extension on ϕ_b is found for the 50%NH_3 flame when increasing S. Four flame macrostructure modes can be identified when decreasing equivalence ratio (ϕ). The transition from flame II to flame III (ϕ_t describes the transition equivalence ratio) can be considered as the early warning of blow-off for a swirl stabilized flame. It is found that for the NH_3 flame, there is no clear flame macrostructure transition at small inlet velocities ($U < 3.8$ m/s), i.e., $\phi_b \approx \phi_t$, while the difference between ϕ_b and ϕ_t will be observed as the inlet velocity increases. However, for the 50%NH_3 and CH_4 flames, a clear flame macrostructure transition from flame II to flame III is observed even for a lower inlet velocity. The LES results show that the NH_3 flame has a faster blow-off process compared to the CH_4 flame, which is mainly attributed to the excessive stretch causing local extinction during the blow-off process.

Keywords: Ammonia; Hydrogen carrier; Carbon-free fuel; Lean blow-off; Swirl combustor

1. Introduction

It is well recognized that ammonia (NH_3) combustion could help to achieve zero carbon emission [1,2], because ammonia is not only a suitable hydrogen carrier made up of 17.8 % hydrogen

* Corresponding author.
E-mail address: mengz8851@xjtu.edu.cn (M. Zhang).

https://doi.org/10.1016/j.proci.2020.08.056

by weight but also is a carbon-free molecule [3–5]. Moreover, the production, storage and carriage of ammonia have already been well-established [5], since it is a standard industrial chemical. Therefore, in order to realize low or zero carbon emission, the application of ammonia on modern combustion devices becomes one of the main objectives for the ammonia research community [4–6].

Due to the special characteristics of the ammonia/air flame, i.e., very low laminar flame speed S_L [7] and smaller heat release rate (HRR), it is quite challenging to stabilize the ammonia/air flame in gas turbines. For example, the laminar flame speed of ammonia/air flame is only one fifth of methane/air flame at the stoichiometric condition. And the effect of radiation heat loss on flame speed of the ammonia/air flame is more pronounced compared to the methane/air flame [8]. These features result in ammonia/air flames exhibiting very poor stabilization limits for both premixed and non-premixed combustion modes. Moreover, the flame residence time for ammonia in a gas turbine chamber is relatively long owing to its very small S_L. As a result, a longer combustion chamber is required to stabilize ammonia/air flames at the same inlet velocity compared with traditional hydrocarbon fuels [9], i.e., CH_4/air flame, even for premixed cases [4]. These issues bring great challenges in the application of ammonia in current combustion devices.

Though a non-swirling ammonia/air flame is prone to blow-off due to its weak combustion intensity [4], recent studies have demonstrated that the ammonia/air flame could be successfully stabilized in a swirl combustor [5,10] in the context of a limited equivalence ratio (ϕ) range. Some investigations suggest that the blow-off issue can be overcome through changing the fuel-air mixing type and swirler geometry [3,10]. Nevertheless, a swirl-stabilized flame is prone to local extinction and reignition during the equivalence ratio decreasing operation from a lean stable condition to blow-off. Previous studies proposed that blending ammonia with other active fuels like methane (CH_4) or hydrogen (H_2) can extend its stable combustion range [1,5], since the flame speed, heat release rate and extinction strain rate are increased. These flame properties can play crucial roles in the blow-off behavior as well as the flame macrostructure transition as the equivalence ratio deviates towards the lower stabilization limit. However, the blow-off mechanism and its relation to the flame macrostructure transition and the blow-off behavior for ammonia are not fully understood and hence needs further investigations.

Based on the above considerations, this work aims to reveal the blow-off characteristics and the flame macrostructure transition of the NH_3/air and NH_3/CH_4/air swirling flames through the analysis of flame structures and flow fields near the blow-off limit. The experiments are performed in an updated swirl combustor used in our former studies [11]. Planar Laser Induced Fluorescence (PLIF) technique as well as a digital camera are utilized to detect the instantaneous OH profile and the flame macrostructure. The hot gas velocity field is measured by Particle Imaging Velocimetry (PIV). To further reveal the effect of heat release rate (HRR) and flame stretch on the blow-off process, large eddy simulation (LES) with a dynamic thickened flame model (DTF) [12] based on OpenFOAM is performed to extend understandings of the experimental results.

Table 1
Parameters of the swirler.

Swirler	D_i (mm)	D_o (mm)	θ (°)	Vanes	S
Type1	13	35	30	12	0.42
Type2	13	35	45	12	0.73
Type3	13	35	60	12	1.27

2. Experimental facilities and numerical method

2.1. Experimental setup

A stainless steel, fully premixed swirl combustor is employed in the experiments to stabilize the flame. Figure 1(a) and (b) show the schematic of the combustor head section, the liner and the swirlers used in the experiments. The overall geometry is similar to that used in our previous studies, which can be found in Ref. [11,13]. The main addition to the previous swirl combustor is the liner, which confines the flame. Fuel and air are fully premixed in the mixing section of the burner. Then the mixture goes through a venturi nozzle to prevent the propagation of downstream pressure waves. A perforated plate is installed just after the venturi nozzle to rectify the flow. Furthermore, the swirler is installed just below the burner exit. A squared liner equipped with quartz glass on four sides is used to view the flame and to allow laser diagnostics, as shown in Fig. 1(b). Three types of copper swirlers with 12 vanes, shown in Fig. 1(b), are used to generate swirl flow with different swirl number S, which is calculated by $S = \frac{2}{3} \cdot \frac{1-(D_i/D_o)^3}{1-(D_i/D_o)^2} \tan\theta$ [14]. θ represents the vane angle. The diameters of the burner and swirlers are summarized in Table 1.

The fuel and air mass flow rates are precisely controlled through SevenStar flowmeters (CS230, CS200) with a relative error smaller than $\pm 1.5\%$ of the measuring range. The composition of the mixture and the operating conditions are listed in Table 2, in which ϕ_b represents the blow-off equivalence ratio and U_{max} is the maximum inlet velocity. For brevity, three flames will be mentioned with their abbreviations in the following text, as designated in Table 2. The NH_3 flame and $50\%NH_3$

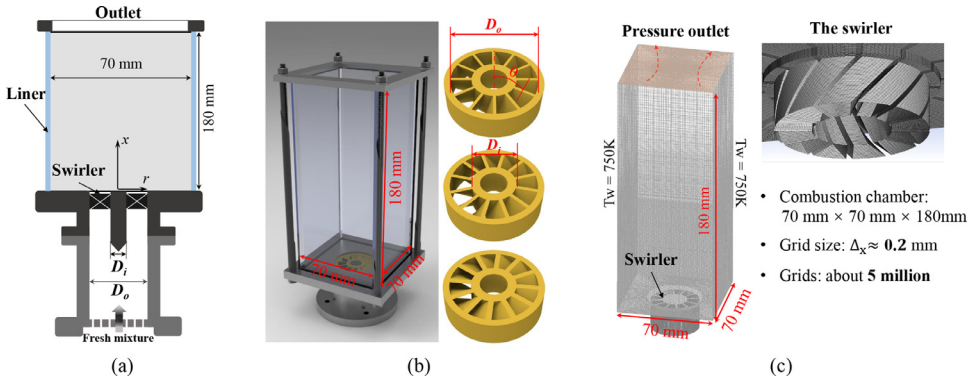

Fig. 1. (a) The schematic of head section of the swirl combustor; (b) the liner and the swirlers; (c) the mesh of computational domain and swirler.

Table 2
Operating conditions in the current study.

Abbreviation	Composition by mole	ϕ	U_{max} (m/s)
CH_4 flame	100%CH_4	0.7-ϕ_b	13
50%NH_3 flame	50%CH_4+50%NH_3	0.74-ϕ_b	13
NH_3 flame	100%NH_3	0.8-ϕ_b	5

flame are investigated for blow-off behavior and both will be compared with the results of the CH_4 flame.

The hot gas velocity and OH profile are measured by PIV and OH-PLIF techniques, respectively. The PIV laser source consists of a double-cavity Nd:YAG laser (Litron make) with a wavelength of 532 nm, 2 × 300 mJ pulse energy at a 10 Hz repetition rate. TiO_2 with a particle size of 0.5–1 μm is used as the seeding particle. A double shutter CCD camera (Imager LX 2M) with the resolution of 1600 × 1200 pixels and minimum 200 ns time separation is used to capture the dual frame of the particle movement, for calculating cross correlation. The scattering is collected by the CCD with a macro lens (100 mm, F/2.8) at a working distance of 400 mm, filtered with a narrow bandpass filter (LaVision, 532 ± 5 nm, a bandwidth of 10 nm). The OH-PLIF system mainly includes a Nd:YAG laser (Quanta-Ray Pro-190), a pumped dye laser (Sirah PRSC-G-3000), an ICCD camera (LaVision Image ProX) and the data acquisition software. The source laser is generated at a wavelength of 532 nm, 10 Hz and the power of 5 W. The laser frequency is doubled with the pumped dye laser and the wavelength is transferred to 282.769 nm to excite the Q1(8) line of the $A2\Sigma \leftarrow X2\Pi(1, 0)$ transition. A 0.5 mm thick laser sheet with 80 mm in height is formed through the optical elements. The OH fluorescence from the (0,0) band (around 308 nm) is detected by an ICCD camera through a UV lens (Nikon Rayfact PF 10545MF-UV) with intensified Relay Optics (LaVision VC08-0094) and a OH bandpass filter (LaVision VZ08-0222). The resolution of the OH-PLIF image is 1200 × 900 pixels with the pixel size of 0.14 mm/pixel. The direct flame images are recorded by a Cannon Kiss X5 camera with a prime lens (EF 50mm, f/1.4 USM) to capture the mean flame status.

2.2. Numerical methodology

LES with a finite rate chemistry based on OpenFOAM is performed on the same burner geometry as the experiment to further reveal the mechanisms of blow-off. The simulation solves the filtered 3D unsteady conservation equations of mass, momentum, energy as well as the state equation. An updated dynamic thickened flame (DTF) model is applied by introducing a thickening factor (F) into the species equations. To resolve the flame structure with a coarse mesh, the flame is artificially thickened by a factor of F while keeping the laminar flame speed S_L unchanged. A subgrid flame wrinkling factor Ξ_Δ based on fractal theory is included [15] to account for the unresolved flame wrinkling due to the thickening process. The chemical source term and the diffusion term are modified by F and Ξ_Δ. Detailed information on the DTF model can be found in the Supplementary Material and our previous studies [12,13].

The computational domain mainly includes two sections, namely the combustion chamber and the swirler section. The dimension of the combustion chamber is 70 × 70 × 180 mm^3 as shown in Fig. 1(c). A 12-vane axial swirler with a vane angle of 45° is meshed to directly simulate the swirl flow. The overall computational domain is divided into 274 blocks and contains about 5 million structured grids with a minimum grid spacing of 0.2 mm at the flame location. We carefully tested the current mesh by further refining the mesh and found that the refinement did not affect the statistics of the flow field. In the DTF model, the thickening factor

(F) is usually chosen with 4 $\sim$ 6 points resolving the reaction layer. Therefore, $F = 3$ is applied based on the laminar flame thickness of methane/air at $\phi = 0.6$ in this work. The isothermal wall of T_{wall} = 750 K is applied for the liner walls, which is obtained from the averaged value of experimental measurements. The adiabatic boundary is applied for the burner outlet. Pressure outlet is applied at the exit of the chamber which is verified adequately by capturing the flow in the combustion chamber, see Section 3.4. In the present simulation, the temperature of the inlet mixture and the ambient pressure are 300 K and 1.0 atm, respectively. The total mixture flow rate is maintained constant at 150 LPM for every case. Flame properties of one-dimensional laminar flame are obtained through ANSYS Chemkin-PRO [16]. Both LES and laminar flame calculations are performed using the chemical mechanism of methane/ammonia/air developed by Okafor et al. [17] with 59 species and 368 reactions. With the current mesh, each LES case requires approximately 0.32 million CPU hours.

3. Results and discussions

3.1. The flame properties

The flame macrostructure and blow-off behavior are highly influenced by flame properties which are significantly different for the three flames listed in Table 2. The extinction strain rate K_{ext}, laminar flame speed S_L, adiabatic flame temperature T_{ad}, the laminar flame thickness δ_L as well as the maximum heat release rate HRR are compared for the three flames, see the Supplementary Material. K_{ext} and S_L of the NH_3 flame are significantly smaller than that of the CH_4 flame, resulting in more easily extinguishing for the NH_3 flame. Due to smaller S_L, NH_3 needs to be stabilized at low mean bulk velocity [10]. Moreover, the maximum heat release rate, calculated from the one-dimensional flame, of the NH_3 flame is lower than that of the CH_4 flame. This indicates that the heat loss effect on combustion intensity, i.e. laminar flame speed, will be more significant for the NH_3 flame, as shown in Ref. [8]. Overall, the slow and weak combustion of ammonia will cause new issues of flame stabilization in swirl combustors. It is apparent that the properties of ammonia for both laminar and swirling flames can be manipulated by blending it with methane, which will be presented and discussed in the subsequent sections.

3.2. The blow-off characteristics

Figure 2 shows the direct image and the flame structure overlapped with mean velocity field for the three flames. LES is conducted for the NH_3 and CH_4 flames, also shown in Fig. 2 for comparison. The recirculation zones and shear layers are clearly seen from the mean velocity field, as indicated in Fig. 2. Due to slower S_L, the residence time for the NH_3 flame is longer, resulting in a higher flame. Because the NH_3 flame cannot be stabilized at as high of a inlet velocity (U) or lean condition as the CH_4 flame, the CH_4 and 50%NH_3 flame are stabilized at $\phi = 0.6$ and $U = 5$ m/s while the NH_3 flame is stabilized at $\phi = 0.7$ and $U = 4$ m/s in our experiment.

Moreover, it can be observed that the required combustion chamber length is reduced as a result of the decreasing flame length when the flame is blended with methane. The flame cannot be seen in the outer recirculation zone (ORZ) for the NH_3 flame compared with the CH_4 flame, indicating ORZ does not contribute to the flame stabilization [18]. This is because the flame (or the hot gas) in ORZ can hardly be formed in the lean condition due to the lower heat release rate. It can be observed from surveying the OH-PLIF images that the OH intensity of the NH_3 flame is weaker compared with the CH_4 flame. In addition, the finest scale of the flame front wrinkles is larger for the NH_3 flame (also seen in Fig. 4). This is due to its larger preheating zone thickness since the flame front still maintains the flamelet structure, see the turbulent flame regime in the Supplementary Material.

We next test the lean blow-off limits (blow-off equivalence ratio ϕ_b) for the three flames. ϕ_b is highly affected by the flow conditions for each fuel and the $U \sim \phi_b$ relation defines the lean boarder of the stable combustion at various inlet velocities [3,10]. ϕ_b is obtained by gradually increasing the mass flow rate of air at a constant fuel mass flow rate until the flame is blown away. Then the flow rates of air and fuel are recorded to calculate the blow-off equivalence ratio ϕ_b. This procedure is repeated with increasing the flow rate of fuel to obtain the lean blow-off limits curve for each swirler ($S = 0.42, 0.73, 1.27$), as shown in Fig. 3. For the CH_4 flame, only the result of $S = 0.73$ is shown for the purpose of comparison.

It is clear that the NH_3 flame possesses very poor lean flame stability limits compared to the CH_4 flame. And the change in swirl number shows no apparent effect on extending the blow-off limit of the NH_3 flame for the current burner. As shown in Fig. 3, the lean blow-off limits are roughly close for each S, i.e. $\phi_b \approx 0.65$. When $S = 0.42$, large flame fluctuations are observed during experiments as the flame approaches blow-off limits, which may induce combustion oscillations. However, no visible flame fluctuation is seen for the flames under the condition of $S = 0.73$ and 1.28. In comparison, it is readily seen that the blow-off limits can be primarily extended by adding 50% methane into the fuel. Moreover, unlike the NH_3 flame, an obvious extension on the lean blow-off limit is seen for the 50%NH_3 flame when increasing the swirl number. Similar behavior is also seen for the CH_4 flame.

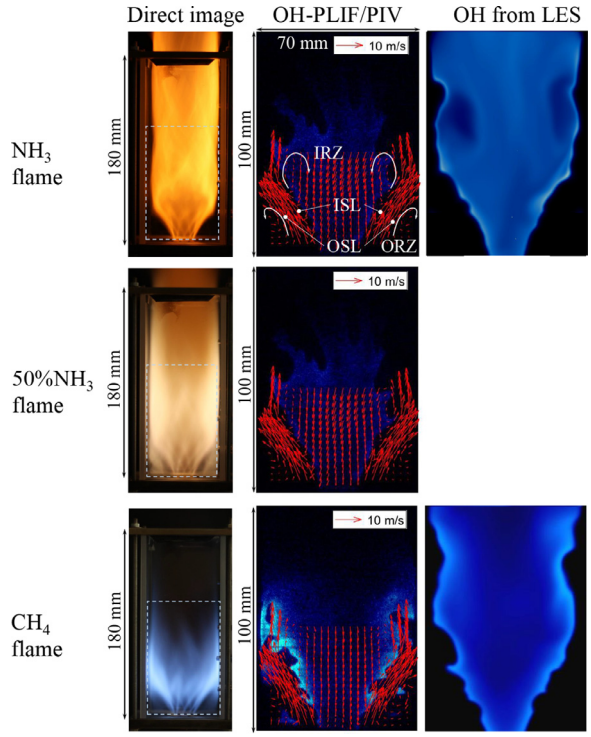

Fig. 2. Top row shows the NH_3 flame at $\phi = 0.7$ and $U = 4$ m/s; middle and bottom rows show the 50% NH_3 flame and CH_4 flame at $\phi = 0.6$ and $U = 5$ m/s respectively. OH-PLIF images are taken within the dashed box and overlapped with the mean velocity field of hot gas. The inner/outer recirculation zone (shear layer) is abbreviated as IRZ/ORZ (ISL/OSL). The orange chemiluminescence of the NH_3 flame is due to the $NH_2\alpha$ band and the super-heated H_2O vapour spectra.

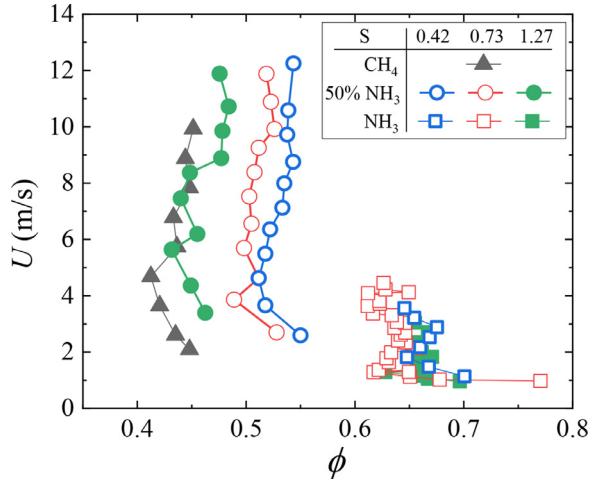

Fig. 3. The blow-off limits ϕ_b for the three fuels. Only the result of $S = 0.73$ for the CH_4 flame is shown for comparison.

3.3. The transition of flame macrostructure

To further clarify the flame characteristics during the equivalence ratio decreasing operation, the instantaneous flame structure, i.e., OH profile, at $S = 0.73$ with ϕ is shown in Fig. 4. The measurements are performed at $U = 5.0$ m/s for the CH_4 flame, 50%NH_3 flame and $U = 4.0$ m/s for the NH_3 flames. The flame macrostructure transition is clearly seen and the difference between these

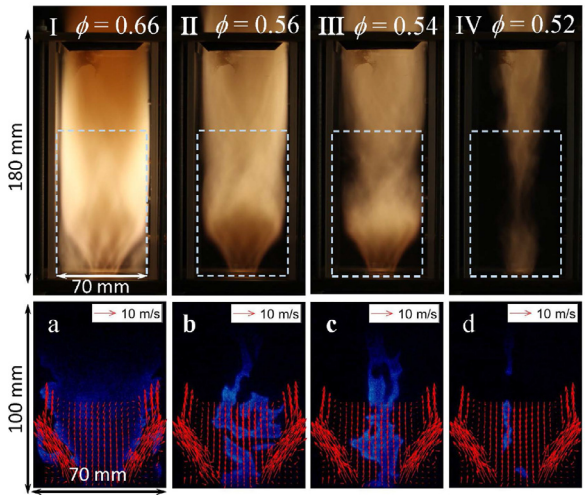

Fig. 5. The flame transition from a stabilized lean condition to blow-off limit for the 50%NH_3 flame at $S = 0.73$, $U = 5$m/s. Top row: direct flame images, bottom row: OH-PLIF images overlapped with mean hot gas velocity within the dashed box.

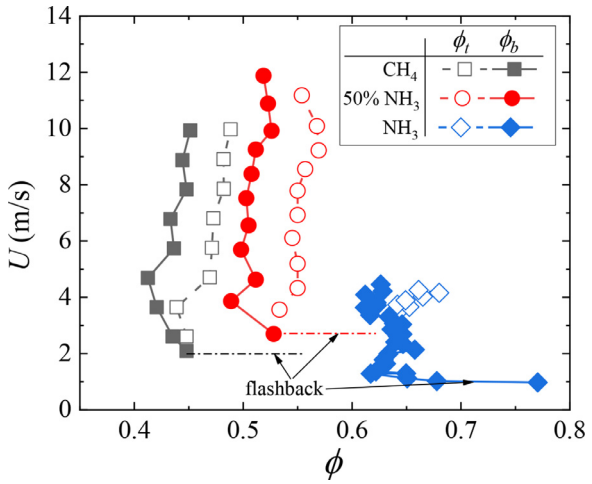

Fig. 6. The flame transition curve ϕ_t along with blow-off limits ϕ_b for the three flames at S=0.73.

three flames are distinct. Since the ϕ increment is small and the mean velocity field is similar, only the OH-PLIF is shown in Fig. 4. The position the inner/outer recirculation zone (IRZ/ORZ) and inner/outer shear layer (ISL/OSL) can be referred to Fig. 2. For the CH_4 flame and the 50%NH_3 flame, as the mixture becomes leaner, the flame in ORZ gradually disappears and then the flame in OSL rolls up. Further decreasing ϕ, local extinction is observed at the flame base and the flame slightly lifts off. Near ϕ_b, the flame is strongly stretched in the shear layer and finally blows away. For the NH_3 flame, however, no flame in the recirculation zone is seen even at $\phi = 0.8$ due to the less intensive combustion. The flame front is less wrinkled compared to the CH_4 flame and the 50%NH_3 flame. The flame structure for S=0.42 and 1.27 shows a similar trend, which is shown in the Supplementary Material due to brevity.

This behavior can be further revealed through the morphology of the flame macrostructure with equivalence ratio ϕ. Figure 5 shows the direct flame images illustrating flame macrostructure with decreasing ϕ, with the instantaneous OH profile overlapped with mean hot gas velocity field beneath it. The flame front can be identified with the sharp boundary of the OH distribution for premixed flames [19]. As observed from the figure, when decreasing ϕ towards ϕ_b, the swirl-stabilized flame will gradually lose the stabilization.

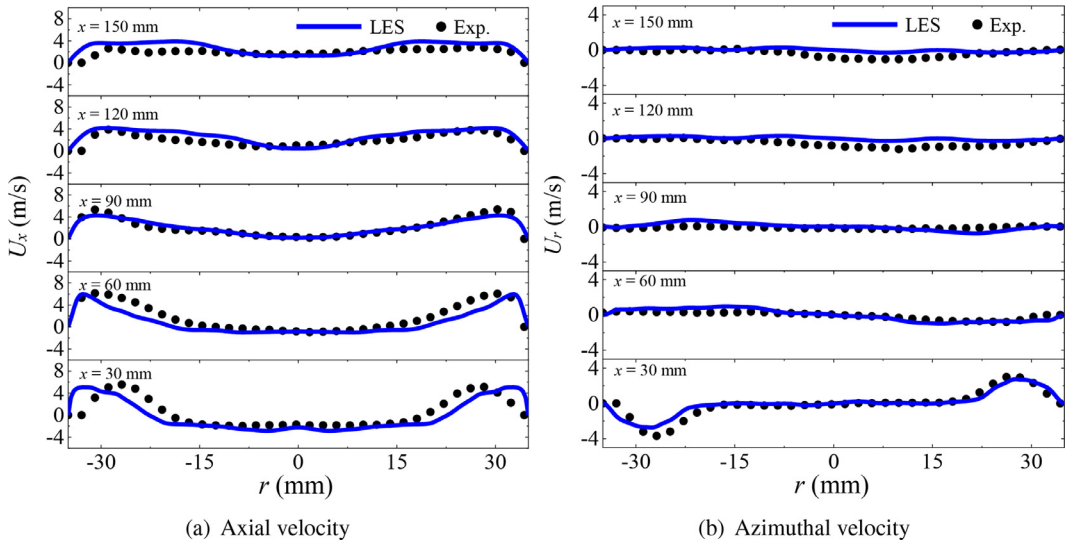

Fig. 7. Comparison of radial profiles of mean axial and azimuthal velocity between LES and PIV measurements for the CH_4 flame at $\phi = 0.6$ and $U = 5$ m/s. Line: numerical results; points: experimental measurements.

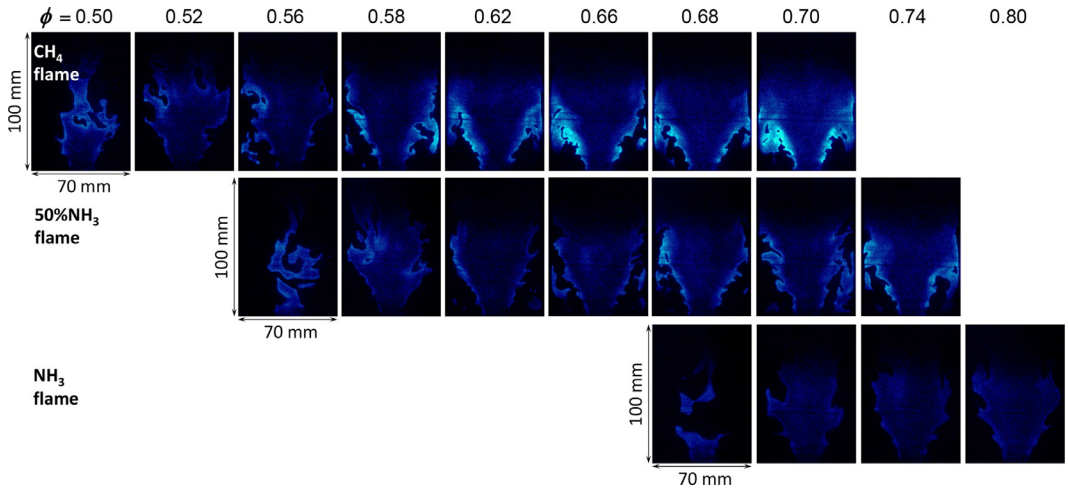

Fig. 4. Instantaneous OH-PLIF images with ϕ from a lean condition towards ϕ_b. Top row: the CH_4 flame; middle row: the 50%NH_3 flame; bottom row: the NH_3 flame. Note that the wall of the combustion liner coincides with the edge of the images shown above.

Four flame macrostructures modes can be identified [20,21] based on the recirculation zones and shear layers. The characteristics and subsequent flame names are described as follows: (a) an "M" shape flame that develops an additional flame in the bottom corner of the chamber, stabilized in the ORZ and along the OSL, is designated as flame I. For flame I, the flamelets (the sharp boundary of OH profile) exist in ORZ which can be clearly observed in the OH-PLIF image; (b) a "V" shape flame which one main flame is detected and stabilized along the ISL is designated as flame II. For flame II, the flame starts to roll up in the shear layer and to be locally extinguished since the flame weakens and is strongly stretched; (c) a bubble flame followed by a columnar flame stabilized in IRZ is designated as flame III. The recirculation of hot gas in IRZ becomes a primary reason for the stabilization of this flame; (d) a lifted flame that is approaching the blow-off limit, is designated as flame IV. In this case, a large number of flame elements are extinguished. When further decreasing the equivalence ratio, no flame will be captured and the flame completely blows away.

The flame macrostructure transition from II to III is crucial and can be viewed as a precursor

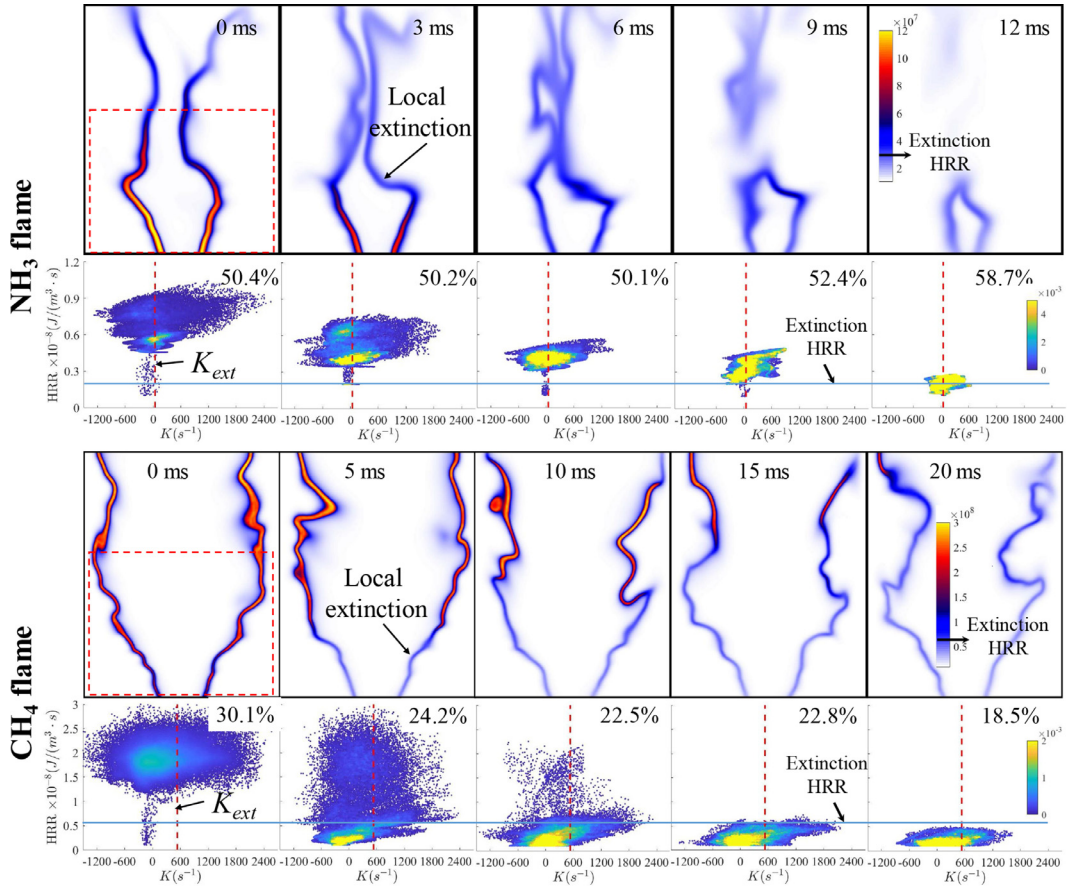

Fig. 8. The time sequences of HRR (top row) and joint PDF of stretch rate and HRR for the NH_3 and the CH_4 flames. The dashed line corresponds to the extinction stretch rate. Image dimensions are 75×90 mm^2. The PDFs are calculated based on the data in the red dashed box. The percentage of the stretch larger than K_{ext} is shown in right conner of the PDF.

event to blow-off as ϕ gradually decreases. Figure 6 shows the flame transition line (ϕ_t) with the blow-off (ϕ_b) curve for $S = 0.73$. The minimum inlet velocity is restricted by the flashback, as indicated in the figure. No clear transition is noticed when U is below 3.8 m/s for the NH_3 flame since the flame is weak and the heat loss is non-negligible. In this case, when the flame starts to extinguish, the whole flame will be blown-off. In the other words, the flame would be suddenly blown away from a stable state, i.e., from flame II. Moreover, the gap between the blow-off and transition curve gradually increases with U when the velocity is above 3.8 m/s. For the CH_4 flame and 50%NH_3 flame, a clear transition event is observed above the U corresponding to flashback. The gap widens at first and remains approximate at a certain value with U. The transition curve can be viewed as the early warning of blow-off on a swirl stabilized flame in the transient operation, which can be used as a guidance in combustor design.

3.4. The stretch effects on blow-off via LES

To further investigate the blow-off process for the NH_3 flame, LES with detailed chemistry is conducted. Firstly, we calculated a stable flame at lean condition near blow-off, namely $\phi = 0.7$ for the NH_3 flame and ϕ =0.6 for the CH_4 flame at $U = 5$ m/s. Figure 2 shows the comparison of the instantaneous OH concentration for both NH_3 flame and CH_4 flame. Also, Fig. 7 plots the radical profiles of mean axial and azimuthal velocities. The statistical data is obtained over 100 ms from the simulation results. From the two figures, it can be seen that the difference between the LES calculation and experiment is minor, showing a good prediction capability on the chemistry, flow dynamics and the proper specifications of the boundary conditions of the current simulation. Secondly, ϕ is impulsively decreased to 0.3 from the aforementioned stable condition to investigate the flame characteristics during blow-off.

Figure 8 shows the flame evolution by heat release rate (HRR) with the joint PDFs of stretch rate and HRR calculated within the red dashed box, with t = 0 ms corresponding to the instance of the change in equivalence ratio. The dashed line plotted in the PDF represents the extinction stretch rate K_{ext}. The HRR region can be regarded as an indicator of the flame. The color bar is adjusted to fit with HRR value based on the maximum HRR for each flame, i.e., 1.2×10^8 J/(m$^3 \cdot$ s) for the NH_3 flame and 3.0×10^8 J/(m$^3 \cdot$ s) for the CH_4 flame. The flame is regarded as extinct if the HRR is smaller than 20% of the maximum value, as indicated in Fig. 8. The blow-off process is apparently different for the two flames which can be observed from the resistance of the heat release after t = 0 ms. For the CH_4 flame, local extinction at the flame base is observed at an early stage due to the decrease in ϕ, resulting in flame lift-off. The flame appears as if it was pushed downstream by the fresh gas. However, for the NH_3 flame at $\phi = 0.7$, the flame itself is extremely unstable since the combustion is too weak, i.e., 2.42 cm/s, and the condition is near to blow-off. Local extinction for the entire flame is observed at an early stage. Furthermore, the whole blow-off process for the NH_3 flame (12 ms) is faster than the CH_4 flame (20 ms). The local extinction near the nozzle during the blow-off process can be attributed to two factors: 1) the flame stretch rate larger than K_{ext} (excessive stretch), 2) the decrease in heat release due to the reduction of equivalence ratio. The flame tends to be extinguished either by encountering the excessive stretch or decreasing HRR below the extinction HRR (HRR_{ext}). The leading cause for extinction is different for these two flames and can be observed from the joint PDFs. As seen from Fig. 8, for the CH_4 flame, the percentage of the excessive stretch is smaller than 30.1% and the HRR is largely decreased below HRR_{ext} at $t >$ 5 ms. This implies that the local extinction near the nozzle is mainly attributed to the HRR decreasing below HRR_{ext}. For the NH_3 flame, the excessive stretch is over 50% in the whole process while nearly all the HRR is above HRR_{ext} until $t = 12$ ms. The results demonstrate that the excessive stretch is the main contribution to local extinction during the transient blow-off process for the NH_3 flame. This indicates that the NH_3 flame should be stabilized with a moderate flow and also explains why the stabilization range of the NH_3 flame cannot be extended through increasing S.

4. Conclusions

This work investigates the blow-off as well as the flame macrostructure transition behavior for both ammonia/air flame (NH_3 flame) and ammonia/methane/air flame (50%NH_3 flame) in a swirl stabilized combustor. The reacting flow field and instantaneous OH profile are measured with PIV and OH-PLIF technique, respectively. LES with DTF model is performed to further understand the experiment results and reveal blow-off mechanisms. The comparison between the LES results and experimental data is in good agreement. It is found that the NH_3 flame possesses a very poor lean flame stability limit compared with the CH_4 flame due to its weak combustion. Moreover, changing the swirl number has a negligible effect on extending the blow-off limit (ϕ_b) for the NH_3 flame. Adding 50% CH_4 in the fuel can widely extend the blow-off limits ϕ_b, which can be further promoted by increasing swirl number for this mixture composition. Four flame macrostructure modes can be identified as the equivalence ratio deceases. ϕ_t describes the transition from flame II to flame III which can be considered as the early warning of blow-off for a swirl stabilized flame. It is found that for the NH_3 flame, no clear flame macrostructure transition is observed at lower inlet velocity (U) due to the weak combustion while the gap between ϕ_b and ϕ_t gradually increases as U goes higher. However, a clear transition event is observed for both 50%NH_3 flame and CH_4 flame. The numerical results from an impulse decreasing equivalence ratio show that the blow-off process of the NH_3 flame is faster than that of the CH_4 flame. Furthermore, compared to the CH_4 flame, the excessive stretch has a more substantial effect on the local extinction for the NH_3 flame during the blow-off process.

Declaration of Competing Interest

None.

Acknowledgements

This study is supported by the National Natural Science Foundation of China (No. 51706172) and the Post Doctoral Foundation of China (2017M613130, 2018T111060).

Supplementary material

Supplementary material associated with this article can be found, in the online version, at doi:10.1016/j.proci.2020.08.056.

References

[1] A. Valera-Medina, H. Xiao, M. Owen-Jones, W. David, P. Bowen, *Prog. Energy Combust. Sci.* 69 (2018) 63–102.
[2] J. Ikheimo, J. Kiviluoma, R. Weiss, H. Holttinen, *Int. J. Hydrogen Energy* 43 (36) (2018) 17295–17308.
[3] E.C. Okafor, K.K.A. Somarathne, A. Hayakawa, T. Kudo, O. Kurata, N. Iki, H. Kobayashi, *Proc. Combust. Inst.* 37 (4) (2019) 4597–4606.

[4] H. Kobayashi, A. Hayakawa, K.K.A. Somarathne, E.C. Okafor, *Proc. Combust. Inst.* 37 (1) (2019) 109–133.
[5] A. Valera-Medina, R. Marsh, J. Runyon, D. Pugh, P. Beasley, T. Hughes, P. Bowen, *Appl. Energy* 185 (2017) 1362–1371.
[6] S. Li, S. Zhang, H. Zhou, Z. Ren, *Fuel* 237 (2019) 50–59.
[7] A. Hayakawa, T. Goto, R. Mimoto, Y. Arakawa, T. Kudo, H. Kobayashi, *Fuel* 159 (2015) 98–106.
[8] H. Nakamura, M. Shindo, *Proc. Combust. Inst.* 37 (2) (2019) 1741–1748.
[9] D. Pratt, Performance of Ammonia-fired Gas-turbine Combustors, *Report*, Berkley University of California, 1967.
[10] A. Hayakawa, Y. Arakawa, R. Mimoto, K.K.A. Somarathne, T. Kudo, H. Kobayashi, *Int. J. Hydrogen Energy* 42 (19) (2017) 14010–14018.
[11] W. Zhang, J. Wang, W. Lin, S. Guo, M. Zhang, G. Li, J. Ye, Z. Huang, *Exp. Thermal Fluid Sci.* 104 (2019) 15–25.
[12] S. Guo, J. Wang, X. Wei, S. Yu, M. Zhang, Z. Huang, *Fuel* 233 (2018) 346–353.
[13] S. Guo, J. Wang, W. Zhang, B. Lin, Y. Wu, S. Yu, G. Li, Z. Hu, Z. Huang, *Appl. Therm. Eng.* 160 (2019) 114021.
[14] Y. Huang, V. Yang, *Prog. Energy Combust. Sci.* 35 (4) (2009) 293–364.
[15] F. Charlette, C. Meneveau, D. Veynante, *Combust. Flame* 131 (1) (2002) 181–197.
[16] CHEMKIN-PRO 17.2, ANSYS, Inc.: San Diego
[17] E.C. Okafor, Y. Naito, S. Colson, A. Ichikawa, T. Kudo, A. Hayakawa, H. Kobayashi, *Combust. Flame* 187 (2018) 185–198.
[18] S. Taamallah, Z.A. LaBry, S.J. Shanbhogue, A.F. Ghoniem, *Proc. Combust. Inst.* 35 (3) (2015) 3273–3282.
[19] M. Zhang, J. Wang, Y. Xie, Z. Wei, W. Jin, Z. Huang, H. Kobayashi, *Exp. Thermal Fluid Sci.* 52 (2014) 288–296.
[20] J.P. Moeck, J.-F. Bourgouin, D. Durox, T. Schuller, S. Candel, *Combust. Flame* 159 (8) (2012) 2650–2668. Special Issue on Turbulent Combustion
[21] C. Foley, I. Chterev, J. Seitzman, T. Lieuwen, Flame configurations in a lean premixed dump combustor with an annular swirling flow, *7th US National Combustion Meeting*, 2011.